JACS
JOURNAL OF THE AMERICAN CHEMICAL SOCIETY
Article
pubs.acs.org/JACS

Heterogeneous Electrocatalyst with Molecular Cobalt Ions Serving as the Center of Active Sites

Jiong Wang,[†,‡] Xiaoming Ge,[§] Zhaolin Liu,[§] Larissa Thia,[†] Ya Yan,[†] Wei Xiao,*[,∥] and Xin Wang*[,†,‡]

[†]School of Chemical and Biomedical Engineering, and [‡]Center for Programmable Materials, Nanyang Technological University, 62 Nanyang Drive, Singapore, 639798

[§]Institute of Materials Research and Engineering (IMRE), Agency of Science, Technology, and Research (A*STAR), 3 Research Link, Singapore, 138632

[∥]School of Resource and Environmental Sciences, Hubei International Scientific and Technological Cooperation Base of Sustainable Resource and Energy, Wuhan University, Hubei 430072, China

Supporting Information

ABSTRACT: Molecular Co^{2+} ions were grafted onto doped graphene in a coordination environment, resulting in the formation of molecularly well-defined, highly active electrocatalytic sites at a heterogeneous interface for the oxygen evolution reaction (OER). The S dopants of graphene are suggested to be one of the binding sites and to be responsible for improving the intrinsic activity of the Co sites. The turnover frequency of such Co sites is greater than that of many Co-based nanostructures and IrO_2 catalysts. Through a series of carefully designed experiments, the pathway for the evolution of the Co cation-based molecular catalyst for the OER was further demonstrated on such a single Co-ion site for the first time. The Co^{2+} ions were successively oxidized to Co^{3+} and Co^{4+} states prior to the OER. The sequential oxidation was coupled with the transfer of different numbers of protons/hydroxides and generated an active Co^{4+}═O fragment. A side-on hydroperoxo ligand of the Co^{4+} site is proposed as a key intermediate for the formation of dioxygen.

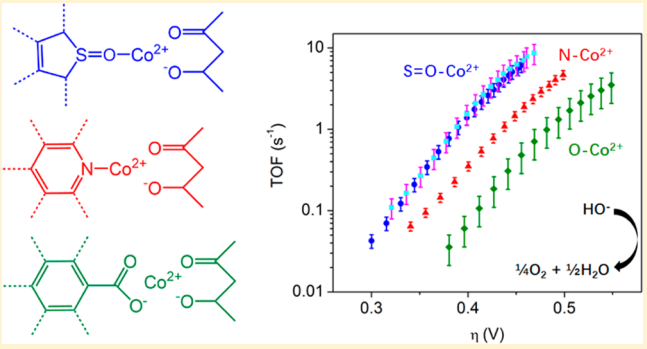

INTRODUCTION

The electrochemical splitting of water into oxygen and hydrogen is a promising approach for sustainable energy conversion, which can potentially reduce our dependence on fossil fuels and alleviate atmospheric pollution.[1−3] The sluggish oxygen evolution reaction (OER) occurring at the anode of a water-splitting electrochemical cell usually requires large overpotentials (η) of 300−500 mV, likely due to the generation of energetic intermediates in the multiple electron and proton coupling steps.[4] Efficient electrocatalysts are required to accelerate the OER in terms of increasing the turnover frequency (TOF) of catalytic sites at low η.[5] In principle, the TOF can be improved by molecular electrocatalysts because their active sites can be fully exposed to reactants and are well-defined to allow systematic tuning of electrocatalytic activity.[6−8] However, molecular electrocatalysts often demand specific solvents to sustain activity, and they are difficult to recover from the reaction medium or to readily integrate into electrolysis systems.[9−11] Immobilizing molecular electrocatalysts onto heterogeneous matrices would be a reasonable approach to overcome such drawbacks. Several recent studies have proposed different approaches to immobilize molecular electrocatalysts onto heterogeneous matrices for a target reaction. Generally, these approaches include confining molecular electrocatalysts within thin films of metal (covalent) organic frameworks[11] and covalently connecting molecular electrocatalysts onto solid surfaces.[12,13] In particular, the latter strategy combined with carbon-based matrices has attracted the most interest because carbon offers many advantages, such as a high surface area, good electrical conductivity, robustness, and appropriate surface functionality to allow constructing versatile covalent linkages at carbon atoms.[12,14,15] The studies further imply that engineering the configurations of electrical wires[13,16] or shortening the distances[11] between active sites and the solid surface is critical to the interfacial electron transfer, thereby enabling tuning of the overall reaction rates.

In the case of OER electrocatalysis, various research studies have shown that Co-based systems are promising. Among these Co-based systems, spinel Co_3O_4 is the most representative. Spinel Co_3O_4 consists of Co_4O_4 cubane and surface-exposed Co^{3+} ions bearing an octahedral configuration.[17−19] Mechanistic insights, gained from either experiments[20,21] or theoretical calculations,[18] have suggested that Co^{2+} cations are converted into Co^{4+} states with dual Co sites to catalyze OER events.

Received: October 4, 2016
Published: January 18, 2017

DOI: 10.1021/jacs.6b10307
J. Am. Chem. Soc. 2017, 139, 1878−1884

On the basis of the aforementioned considerations, we started from molecular Co^{2+} ions and grafted them onto graphene-based matrices. It was found that a single Co^{2+} ion can also serve as the origin of the OER active site instead of the dual Co site. The binding of Co^{2+} ions was accomplished mainly by heteroatoms, i.e., S, N, and O, within graphene. The heteroatoms carry extra electrons compared to neighboring C atoms and provide a coordination environment for the Co^{2+} ions (Figure 1). The effect of various heteroatoms was investigated. In the current configuration, the additional construction of electrical wires or covalent linkages is no longer necessary. The conjugated π electrons of graphene are expected to directly establish the electron communication between Co^{2+} ions and graphene. The synthesis was performed at mild temperatures, which retained the pristine state of Co^{2+} ions without forming other Co-based heterogeneous phases. Our work demonstrates a new type of molecular OER electrocatalyst that is derived simply from Co^{2+} ions and is highly active at the graphene interface. Electrochemical results suggest that the heteroatoms of graphene play an important role in tuning the OER activity. In the presence of a C−S═O fragment, the TOF of Co sites is greatly increased and exceeds the TOF of IrO_2 nanoparticles.[22] We observed the formation of Co^{4+}═O fragments upon sequential oxidation of Co^{2+} ions coupled with H^+ (HO^-) transfer and propose that the Co^{4+}═O fragments served as the single active sites for the electrocatalysis of OER.

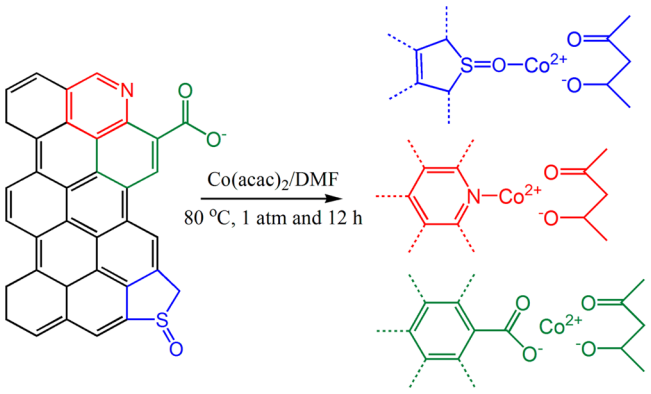

Figure 1. Immobilization of Co^{2+} ions (originating from $Co(acac)_2$) onto S-, N-, O-atom-doped graphene (SNG) using a coordination tether at a mild temperature.

RESULTS AND DISCUSSION

Spectral characterization. Graphene doped with S, N, and O atoms was synthesized from graphene oxide with thiourea as the modifier using a hydrothermal method. SNG was treated with $Co(acac)_2$/dimethylformamide (DMF) solution to obtain the electrocatalyst (denoted as SNG-Co^{2+}). In the meantime, S/O-, N/O-, and O-doped graphene were synthesized to immobilize Co^{2+} ions following the same strategy, which generated three control samples of SG-Co^{2+}, NG-Co^{2+}, and OG-Co^{2+} for comparison (details are provided in the experimental part and in Figure S1, Supporting Information [SI]). Scanning electron microscopy (SEM) and transmission electron microscopy (TEM) imaging combined

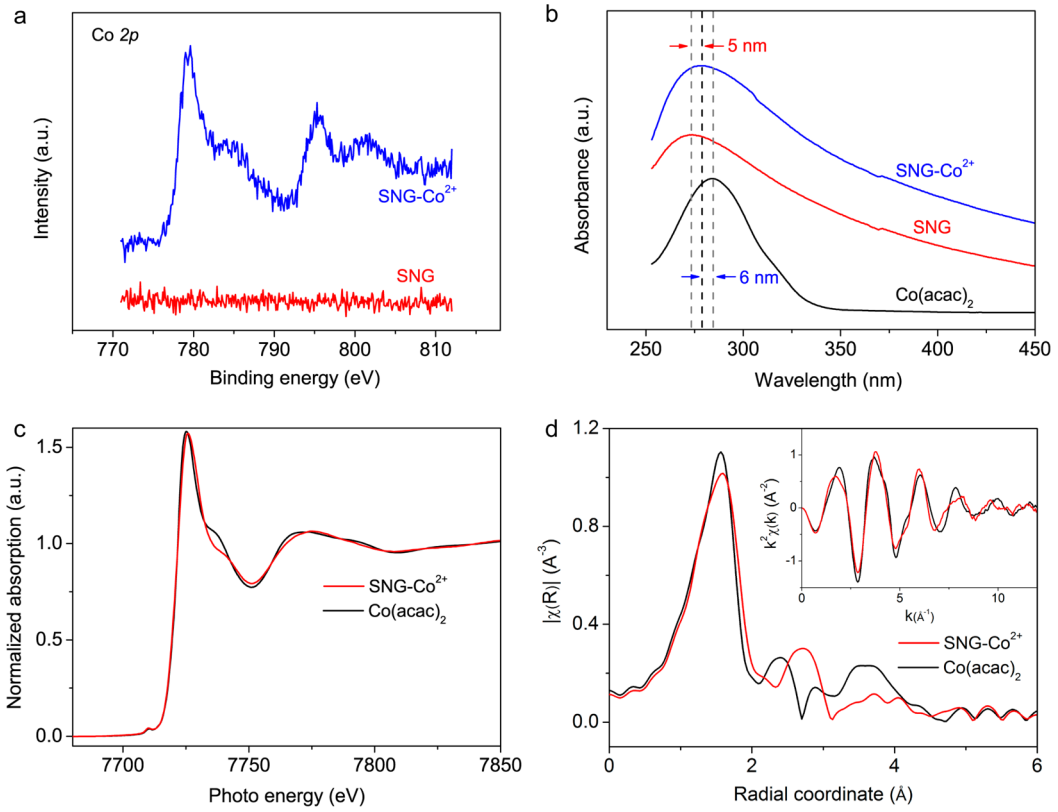

Figure 2. (a) XPS spectra of the Co 2*p* core levels of SNG-Co^{2+} and SNG; (b) UV−vis spectrum of SNG-Co^{2+} collected in ethanol, as compared to the spectra of SNG and $Co(acac)_2$. (c) Normalized Co K-edge XAS spectra for SNG-Co^{2+} and $Co(acac)_2$. (d) Corresponding Fourier transformed EXAFS curve collected at the Co K-edge.

DOI: 10.1021/jacs.6b10307
J. Am. Chem. Soc. 2017, 139, 1878−1884

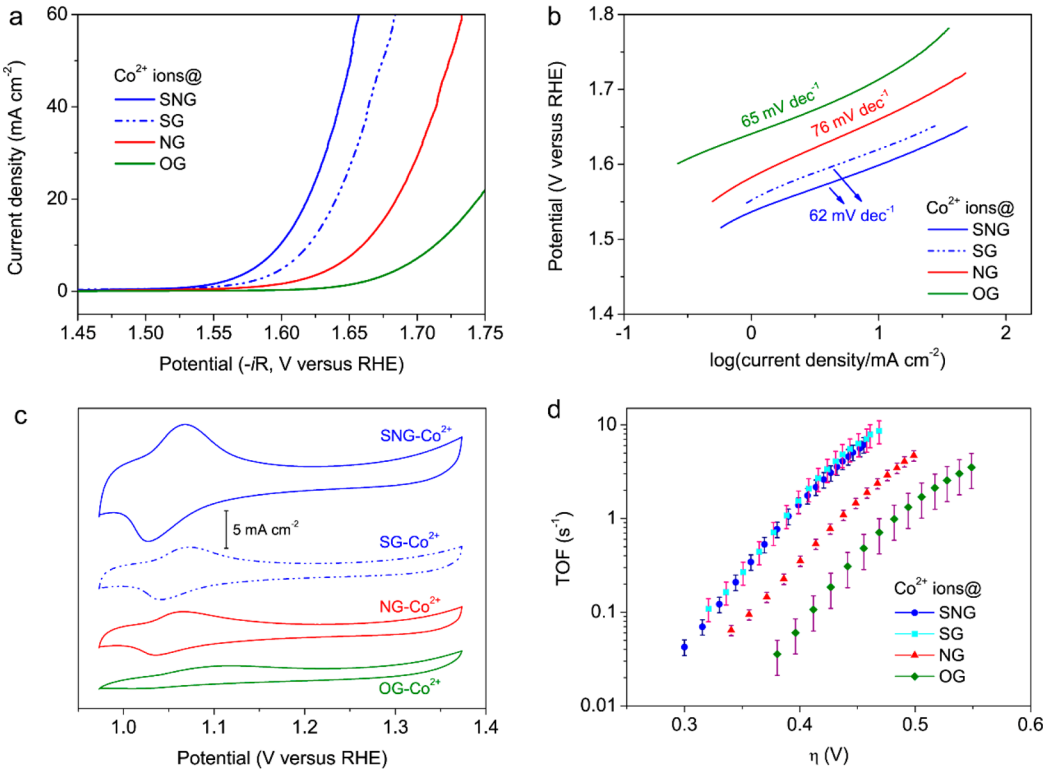

Figure 3. (a) Linear scanning voltammograms (LSVs) of SNG-Co^{2+}, SG-Co^{2+}, NG-Co^{2+}, and OG-Co^{2+}, 1 M KOH, 10 mV s^{-1} scan rate, 2000 rpm. (b) Tafel slopes; the potentials are corrected by *iR* loss and are derived from the OER polarization curves. (c) Cyclic voltammograms (CVs) of Co^{2+} ions on heteroatom-doped graphenes, 1 M KOH, 50 mV s^{-1} scan rate. Each curve was collected using freshly prepared SNG-Co^{2+}/GCE. (d) TOFs of Co sites for OER; the amounts of Co sites on electrodes were determined by integrating the charge amounts of the Co$^{2+/3+}$ oxidation peak.

with elemental analysis revealed the typical graphene character of SNG-Co^{2+}, and Co was observed to be uniformly distributed over the carbon sheets (Figures S2–S4). X-ray photoelectron spectroscopy (XPS) also confirmed the presence of Co species at SNG-Co^{2+} (Figure 2a). Two main peaks occurred at 779.5 and 795.5 eV in an intensity ratio of 2:1, and these peaks were assigned to the Co *2p3/2* and *2p1/2* core levels, respectively. The simultaneous satellite peaks at 785.3 and 801.6 eV indicated the presence of Co in the +2 valence state. From the specific surveys of the S *2p*, N *1s*, and O *1s* core levels (Figure S5), the configurations of heteroatoms of graphene were assigned to (i) thiol (162 eV) and sulfoxide (166.7 eV) groups,[23] (ii) pyridine (397.6 eV) and pyrrole (399.4 eV) groups,[24] and (iii) carboxyl (529.6 eV) and hydroxyl (531.1 eV) groups.[25] UV–vis spectra showed the $\pi-\pi^*$ transition of SNG at 273 nm and the charge transfer of Co(acac)$_2$ at 284.5 nm (Figure 2b). By contrast, the absorbance peak of SNG-Co^{2+} was broadened and centered at 278.5 nm, which suggests the combination of Co^{2+} ions with SNG. Analogous variations of UV–vis absorbance were observed in the spectra of all of the control samples (Figure S6). The Raman spectrum of the SNG-Co^{2+} presented a broad band between 270 and 540 cm^{-1} that was not observed in the spectrum of pristine SNG (Figure S7). The position of this band is consistent with the vibrations of Co–S, Co–N, or Co–O bonds.[26,27] The broad character was indeed not typical compared to the previous Raman characterizations of CoS_x and CoO_x nano-/microstructures,[26] possibly reflecting a continuous state of Co^{2+} ions with different binding configurations.

The formation of SNG-Co^{2+} was further studied by X-ray absorption spectroscopy (XAS). In the normalized Co K-edge spectra, the rising-edge positions of SNG-Co^{2+} and the Co(acac)$_2$ precursor exhibited little difference (Figure 2c) but were clearly distinct from the Co_3O_4 standard and the Co foil (Figure S8). Thus, the overall oxidation state of Co within SNG-Co^{2+} was confirmed to be +2. The Fourier transformed extended X-ray absorption fine structure (EXAFS) data revealed a variation of the neighboring environment for Co^{2+} ions from Co(acac)$_2$ to SNG-Co^{2+} (Figure 2d). The first shell, referring to the bond length of Co–O interactions, was slightly increased, and the peak intensity was decreased. The redistribution of an outer shell for Co^{2+} ions was more obvious than that of the first shell. Simple physical adsorption of Co(acac)$_2$ is excluded because it does not cause such variation of bond length. Electron paramagnetic resonance (EPR) spectra suggested that the coordination geometry of Co^{2+} ions on SNG remained tetrahedral as the configuration of Co(acac)$_2$. But the SNG-Co^{2+} became more EPR-active than Co(acac)$_2$ (Figure S9), indicating the rearrangement of the *d*-filling state in Co^{2+} ions. On the basis of the XAS and EPR analyses, we infer that SNG served as a new ligand to Co^{2+} ions by replacing parts of the acac$^-$ groups and thus immobilized Co^{2+} ions, as proposed in Figure 1.

Electrocatalysis. The OER activity of SNG-Co^{2+} was characterized using a typical three-electrode system. SNG-Co^{2+} was cast onto a glassy carbon electrode (GCE) and was rotated during the experiments to counteract bubble accumulation at the electrode surface. The potential–current polarization curves were recorded after *iR* compensation (where *R* is the serial resistance of the graphene-based electrode, as determined from an AC impedance measurement; see experimental part in the SI for details). As shown in Figure 3a, an apparent anodic current

DOI: 10.1021/jacs.6b10307
J. Am. Chem. Soc. 2017, 139, 1878–1884

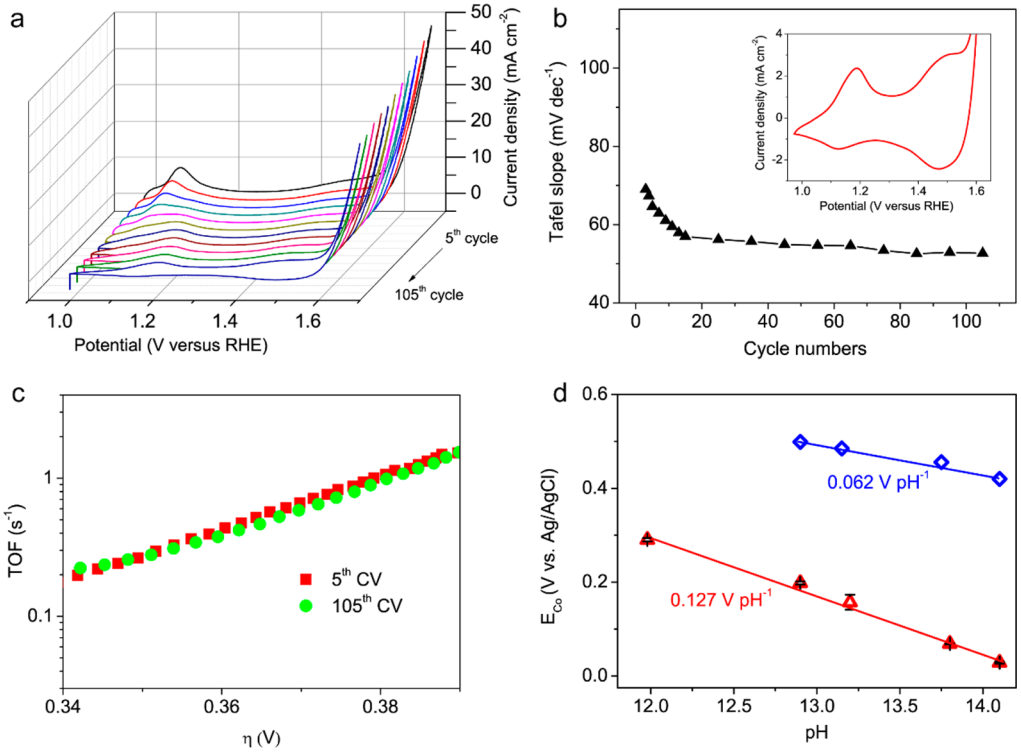

Figure 4. (a) Continuous CV measurements of SNG-Co^{2+}/GCE, 1 M KOH, 50 mV s^{-1} scan rate, 2000 rpm. (b) Tafel slopes derived from the CVs; the potentials were compensated by *i*R; the inset presents the 105th CV of SNG-Co^{2+}/GCE at low potentials. (c) TOFs for the OER derived from the 5th and 105th CVs. (d) Pourbaix diagram (plots of E_{Co} vs pH) of the pH dependence of $Co^{2+/3+}$ redox potentials (red) and reduction potentials of Co^{4+} ions (blue) in KOH solutions. Each data point was collected on a freshly prepared SNG-Co^{2+}/GCE.

occurred at SNG-Co^{2+}/GCE, with an onset potential of 1.6 V (defined as the potential @10 mA cm^{-2} vs the reversible hydrogen electrode, RHE). By contrast, the onset potential increased stepwise when SG-Co^{2+}, NG-Co^{2+}, and OG-Co^{2+} were used. In the corresponding Tafel plots, both SNG-Co^{2+} and SG-Co^{2+} exhibited a lowest linear slope of 62 mV dec^{-1}, closely approaching 59 mV dec^{-1}, corresponding to *2.3 RT/F*, where *R* is the universal gas constant, *T* is the temperature in Kelvin, and *F* is the Faraday constant (Figure 3b). This result implies that a reversible electron transfer occurred prior to the rate-determining step of the OER.[28] At 1.0−1.1 V, a pair of redox peaks was observed for the four electrocatalysts; these peaks were attributed to the $Co^{2+/3+}$ couple (Figure 3c).[29,30] By integrating the charge amounts of the anodic peaks, we obtained the amounts (*m*) of electroactive Co^{2+} ions in the graphene matrices, which are 1×10^{-7}, 2.6×10^{-7}, 2×10^{-7}, and 5×10^{-7} mol per mg of OG, NG, SG, and SNG at GCE, respectively.

To verify that the OER activity originated from SNG-Co^{2+}, we performed a control experiment where SNG-Co^{2+} was treated with an ethylenediaminetetraacetic acid (EDTA)/KOH aqueous solution. Because of the strong chelating ability of EDTA, Co^{2+} ions are displaced from SNG-Co^{2+} to form an EDTA−Co complex in the solution (Figure S10a, b). After the treatment, the UV−vis spectrum of the EDTA/KOH solution showed the characteristic absorbance of an EDTA−Co complex at 534 nm (Figure S10c). Following the Beer−Lambert law, the intensity of absorbance (I = 0.063, ε = 331 M^{-1} cm^{-1})[31] corresponded to a loading amount of Co of the magnitude of 10^{-7} mol/mg_{SNG}, which is consistent with the value calculated from the anodic charge amount of $Co^{2+/3+}$ redox in Figure 2c. With the detachment of Co^{2+} ions, the bare SNG lost the redox feature of $Co^{2+/3+}$. The anodic current dropped substantially and approached zero at potentials lower than 1.67 V (Figure S10d). Therefore, toward the anodic current collected on SNG-Co^{2+}/GCE, the contribution of currents originating from either OER electrocatalysis by SNG or from oxidation of carbon matrices was trivial, and the presence of Co^{2+} ions was critical.

To identify which binding site offers the most active catalytic site, a comparison should be conducted by normalizing the activity with the electroactive Co surface area, i.e., via TOF analysis. Therefore, the specific OER activity of various catalysts was assessed in terms of TOF according to the following equation:

$$\mathrm{TOF} = (J \times A)/(4 \times F \times m) \quad (1)$$

where J is the anodic current density, A is the geometrical surface area of the electrode, F is the Faraday constant, and m is the amount of Co^{2+} ions.

From the TOF analysis, N indeed offers a certain improvement in the OER activity by comparing OG-Co^{2+} and NG-Co^{2+} (Figure 3d and Table S1). However, we also found that SG-Co^{2+} exhibited a much higher TOF than NG-Co^{2+}, clearly indicating that the S-containing group is much more effective in improving the OER activity than the N-containing group. In the case of SNG-Co^{2+}, in addition to such an intrinsic (site-specific) activity difference between N and S, the content of S is much higher than the content of N (the atomic ratio of S/N is approximately 4.5; see Table S2). Therefore, the effect of N on improving OER activity is insignificant compared to the effect of S, which also explains why the TOF of SNG-Co^{2+} is similar to the TOF of SG-Co^{2+} (0.266 s^{-1} vs 0.268 s^{-1} at η of 0.35 V). Therefore, we speculate that the S-containing groups within graphene supply appro-

DOI: 10.1021/jacs.6b10307
J. Am. Chem. Soc. 2017, 139, 1878−1884

priate coordination environments for Co^{2+} cations to make them the most electroactive and are the active sites to catalyze subsequent electrocatalytic reactions. The TOFs of both SNG-Co^{2+} and SG-Co^{2+} exceed those of many previously reported Co-based nanostructures and IrO_2 catalysts (Table S1).

Regarding the binding sites of Co^{2+} ions, in addition to heteroatom sites, the carbon skeleton of graphene might also immobilize Co^{2+} ions via cation−π[32] or van der Waals forces. To eliminate such possibilities, we synthesized another control sample, graphite-Co^{2+}, using the same procedures as for SNG-Co^{2+} because graphite has surface properties similar to intact graphene.[33] Considering that graphite has a much lower specific surface area, its concentration used for the synthesis of graphite-Co^{2+} was multiplied 10-fold compared to the SNG-Co^{2+} case. Electrochemical tests indicated that the redox of $Co^{2+/3+}$ ions on graphite-Co^{2+} was barely detectable and that the OER current was negligible compared to the OER current of SNG-Co^{2+} (Figure S11); these results suggest that the binding of Co^{2+} ions to graphene was accomplished mainly through the heteroatoms. Their configurations within SNG-Co^{2+}, SG-Co^{2+}, NG-Co^{2+}, and OG-Co^{2+} were further compared via XPS analysis (Figure S12). The O *1s* core levels in these four samples exhibited little difference in binding energies. As suggested by the relatively low TOFs of OG-Co^{2+}, the oxygen groups were not likely responsible for the Co-based activity. The S *2p* survey spectra show a peak at 166.7 eV for both SNG-Co^{2+} and SG-Co^{2+}, where these two samples afforded high TOFs. Meanwhile, the NG-Co^{2+} contained obvious N-containing groups, as inferred from its strong N *1s* core levels, but such N-containing groups did not improve TOF to exceed those of SNG-Co^{2+} and SG-Co^{2+}. XPS spectra of graphene-based precursors were also collected. The S *2p* signal at 166.7 eV occurred on both SNG and SG. In the meantime, SNG and NG exhibited similar N *1s* core levels (Figure S13). Combining the results from spectral characterization and electrochemical characterization, we deduce that Co^{2+} ions combined with a sulfoxide (C−S═O) configuration within the graphene are responsible for the most efficient OER active sites.[29,34,35]

Mechanistic insights. Previously, Co_3O_4 was proposed to catalyze OER by forming a Co^{4+}-oxo coordination on dual Co sites.[18] This mechanism is very different from our current system, where the above physical characterizations suggest the molecular state of Co cations on carbon, leading us to regard a single Co site as the origin of the active site. Thus, far, very few mechanistic insights for a single Co site for OER have been reported.[36] To obtain a better understanding of the relevant mechanism, we conducted a series of experiments.

Figure 4a presents continuous CVs of SNG-Co^{2+}/GCE in a wide potential range (0.97−1.67 V). Two peaks were observed in the forward scan before the oxygen evolution. The first peak at 1.1−1.2 V was attributed to Co^{2+}-to-Co^{3+} conversion, and the second peak occurring at 1.4−1.5 V was assigned to the $Co^{3+/4+}$ couple.[37] The derived Tafel slopes of OER gradually decreased and approached ∼52 mV dec^{-1} (Figure 4b), reflecting the reversible electron transfer on the catalyst prior to OER. With the continuous CV scanning, the $Co^{2+/3+}$ redox potential gradually shifted to more positive values, indicating that a stronger electron withdrawing effect occurred on Co^{2+} ions, resulting from the varied coordination.[38] Because the CVs of SNG-Co^{2+}/GCE performed in a low potential range (0.97−1.55 V, Figure S14) still presented the potential shift of $Co^{2+/3+}$, the varied coordination of Co^{2+} ions should not be due to OER polarization. Instead, the varied coordination might imply that a ligand on the Co^{2+} ions was intrinsically labile. Nevertheless, the sequential conversion of Co cations from +2 to +4 valence states remained prominent (Figure 4b inset). The corresponding X-ray diffraction (XRD) pattern did not present any characteristics of possible Co oxides formed from the oxidation of Co cations at the OER potentials (Figure S15). TEM with elemental mapping images also did not suggest the aggregation of Co cations, and the distribution of Co on SNG remained uniform like the case of fresh SNG-Co^{2+} (Figures S4 and S16). Some particles on SNG-Co^{2+} after OER polarization were believed to be carbon fragments because their fringe characters showed little difference compared to the neighboring carbon sheet under higher magnification. In addition, the TOFs also barely changed from the fifth to the 105th CV (Figure 4c). On the basis of these considerations, we deduce that the Co cations remained molecularly dispersed over SNG after the OER and that SNG-Co^{2+} proceeded through a sequential valence conversion: $Co^{2+} \rightarrow Co^{3+} \rightarrow Co^{4+}$. Additionally, the OER stability of SNG-Co^{2+} was examined as a function of time (>10 h), and a less than 5% decrease in the anodic current was observed (Figure S17).

To gain further insight into the formation of actual active sites, the pH dependence of the redox potentials of Co cations on SNG-Co^{2+} was examined in aqueous solutions with different concentrations of KOH (∼12 ≤ pH ≤ 14). Two linear curves, as plotted in a Pourbaix diagram (Figure 4d), were obtained, and their slopes were fitted by the Nernst equation:

$$E = E^{\circ\prime} + 2.3RT/nF \times \log(a_{H+})^b \quad (2)$$

where E ($E^{\circ\prime}$, standard) is the half-cell potential for the Co species, R is the universal gas constant, T is the temperature in Kelvin, n is the number of electrons transferred, and a_{H+} and b are the chemical activity and the stoichiometric number of protons, respectively. In different KOH solutions, the formal potential of $Co^{2+/3+}$ varied by 0.127 V pH^{-1} (blue line), corresponding to a $H^+(HO^-)/e$ stoichiometry of 2 (the standard value = $0.059/n$). For the redox couple of $Co^{3+/4+}$, the reduction potentials were used for the fitting (red line) because the oxidation peaks in diluted KOH solution were ill-defined. The linear slope was 0.062 V pH^{-1}, corresponding to a $H^+(HO^-)/e$ stoichiometry of 1.

Furthermore, from the UV−vis spectra, the absorbance of SNG-Co^{2+} in the UV region showed a blue shift after CV cycles in either the absence or the presence of OER polarization (Figure S18a). Because of the π^* orbitals in both SNG and $acac^-$ (as the counteranions of Co^{2+} ions from the $Co(acac)_2$ precursor), the spectra of SNG-Co^{2+} contained a typical metal-to-ligand charge-transfer (MLCT). The blue shift indicates that the electron transfer from Co^{2+} ions to ligands required a higher excitation energy, consistent with the positive shift of the $Co^{2+/3+}$ potential. Therefore, ligand variation on the Co^{2+} ions likely occurs during the CV cycles. We speculated that, in the KOH electrolyte, HO^- ions, as the other available counter-anions for Co^{2+} ions, replaced the $acac^-$ sites of pristine SNG-Co^{2+} (Figure S18b). The HO^- ions do not contain π^* orbitals to support the MLCT, which explains the blue shift observed in Figure S18a.

On the basis of experimental observations combining with previous quantum chemical models from density functional theory calculations,[36,39] we attempted to deduce a pathway for the evolution of the Co-cations-based molecular catalyst toward the OER (Figure 5). The CVs, in combination with the Pourbaix diagram, indicate that Co^{2+} ions were sequentially

DOI: 10.1021/jacs.6b10307
J. Am. Chem. Soc. 2017, 139, 1878−1884

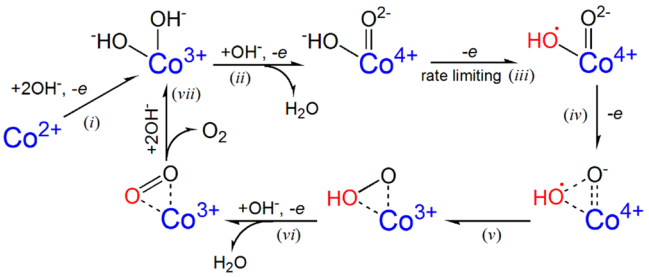

Figure 5. Sequential oxidation of Co^{2+} ions coupled with H^+ (HO^-) transfer, and a proposed OER mechanism on a single Co-cation-based site in an alkaline solution.

oxidized into Co^{3+} and Co^{4+} states, coupled with transfer of either protons or hydroxides (Figure 4a, d). From the slope analysis, in the first oxidation step, two adjacent HO^- ions served as reactants to chemisorb on one Co^{3+} ion (*i*). One of the HO^- ions deprotonated, with Co^{3+}-to-Co^{4+} conversion, to form a $Co^{4+}{=}O^{2-}$ fragment, where the resultant oxo ligands can stabilize the +4 valence state of Co (*ii*).[40] Diverse reactive oxygen intermediates (hydroxyl radical, peroxide, and superoxide species), possibly involved in OER, were then depicted in a sequence following their chemical reactivity.[41] Because the OER was accomplished in an alkaline aqueous medium, we speculate that a rate-limiting step occurred as the oxidation of HO^- to $HO^\bullet$ radical ($HO^- \rightarrow HO^\bullet + e^-$, E^0 = 1.9 V vs SHE), according to a previous study (*iii*).[4] Following the step (*iii*), the unpaired electron of $HO^\bullet$ was donated to the neighboring oxo ligand to form the hydroperoxo configuration (*iv*). The two separated oxygen atoms were thus bonded to generate a side-on dioxygen ligand of Co cations.[42] When the oxo ligands transformed into dioxygen, the Co^{4+} state became less stable and was reduced to the Co^{3+} state to commence another cycle (*v* to *vii*).

CONCLUSION

In summary, Co^{2+} ions were heterogenized by various heteroatom-doped graphene-based solid matrices and served as the center of OER active sites. The heteroatoms (S, N, and O atoms) of graphene directly functioned as the binding sites to anchor Co^{2+} ions. A C−S=O configuration was demonstrated to substantially increase the TOFs of Co sites, resulting in a TOF greater than that of an IrO_2 catalyst. Unlike conventional Co_3O_4, where dual Co sites are regarded as the active sites, the OER was found to be catalyzed by single Co ions with terminal oxo ligands formed after a sequential conversion of $Co^{2+} \rightarrow Co^{3+} \rightarrow Co^{4+}$ coupled with HO^- (H^+) transfer. We proposed that a side-on hydroperoxo ligand on the Co^{4+} active sites enabled formation of dioxygen. The proposed strategy to synthesize a heterogeneous molecular electrocatalyst is easy to carry out and can be extended to various transition metal ions, which opens a new path for the development of heterogeneous molecular electrocatalysts.

ASSOCIATED CONTENT

Supporting Information

The Supporting Information is available free of charge on the ACS Publications website at DOI: 10.1021/jacs.6b10307.

Experimental procedures, data from SEM/TEM images, Raman, EPR, XRD, XAS, UV−vis spectra and elemental analysis (PDF) (PDF)

AUTHOR INFORMATION

Corresponding Authors

*E-mail: gabrielxiao@whu.edu.cn (W.X.).
*E-mail: WangXin@ntu.edu.sg (X.W.).

ORCID

Xin Wang: 0000-0003-2686-466X

Notes

The authors declare no competing financial interest.

ACKNOWLEDGMENTS

This project was funded by the National Research Foundation (NRF), Prime Minister's Office, Singapore, under its Campus for Research Excellence and Technological Enterprise (CREATE) programme. We also acknowledge financial support from the Center for Programmable Materials, Nanyang Technological University, and the academic research fund AcRF tier 2 (M4020246, ARC10/15), Ministry of Education, Singapore. We especially acknowledge Xing-Hua Xia of the School of Chemistry and Chemical Engineering, Nanjing University, and beamline BL14W1, the Shanghai Synchrotron Radiation Facility, for supporting the beam time.

REFERENCES

(1) Costentin, C.; Robert, M.; Saveant, J.-M. *Chem. Soc. Rev.* **2013**, *42*, 2423.
(2) Faber, M.; Jin, S. *Energy Environ. Sci.* **2014**, *7*, 3519.
(3) Lewis, N. S.; Nocera, D. G. *Proc. Natl. Acad. Sci. U. S. A.* **2006**, *103*, 15729.
(4) Wang, J.; Wang, K.; Wang, F.-B.; Xia, X.-H. *Nat. Commun.* **2014**, *5*, 5285.
(5) Yang, P.; Tarascon, J.-M. *Nat. Mater.* **2012**, *11*, 560.
(6) Liu, Y.; Cheng, H.; Lyu, M.; Fan, S.; Liu, Q.; Zhang, W.; Zhi, Y.; Wang, C.; Xiao, C.; Wei, S.; Ye, B.; Xie, Y. *J. Am. Chem. Soc.* **2014**, *136*, 15670.
(7) Blakemore, J. D.; Crabtree, R. H.; Brudvig, G. W. *Chem. Rev.* **2015**, *115*, 12974.
(8) Kang, P.; Meyer, T. J.; Brookhart, M. *Chem. Sci.* **2013**, *4*, 3497.
(9) Cole-Hamilton, D. J. *Science* **2003**, *299*, 1702.
(10) Choplin, A.; Quignard, F. *Coord. Chem. Rev.* **1998**, *178−180* (Part 2), 1679.
(11) Lin, S.; Diercks, C.; Zhang, Y.-B.; Kornienko, N.; Nichols, E.; Zhao, Y.; Paris, A.; Kim, D.; Yang, P.; Yaghi, O.; Chang, C.; Kim, D. *Science* **2015**, *349*, 1208.
(12) Fukushima, T.; Drisdell, W.; Yano, J.; Surendranath, Y. *J. Am. Chem. Soc.* **2015**, *137*, 10926.
(13) Le Goff, A.; Artero, V.; Jousselme, B.; Tran, P. D.; Guillet, N.; Métayé, R.; Fihri, A.; Palacin, S.; Fontecave, M. *Science* **2009**, *326*, 1384.
(14) Pinson, J.; Podvorica, F. *Chem. Soc. Rev.* **2005**, *34*, 429.
(15) McCreery, R. L. *Chem. Rev.* **2008**, *108*, 2646.
(16) Patolsky, F.; Weizmann, Y.; Willner, I. *Angew. Chem., Int. Ed.* **2004**, *43*, 2113.
(17) Gardner, G. P.; Go, Y. B.; Robinson, D. M.; Smith, P. F.; Hadermann, J.; Abakumov, A.; Greenblatt, M.; Dismukes, G. C. *Angew. Chem., Int. Ed.* **2012**, *51*, 1616.
(18) Plaisance, C. P.; van Santen, R. A. *J. Am. Chem. Soc.* **2015**, *137*, 14660.
(19) Hutchings, G. S.; Zhang, Y.; Li, J.; Yonemoto, B. T.; Zhou, X.; Zhu, K.; Jiao, F. *J. Am. Chem. Soc.* **2015**, *137*, 4223.
(20) Zhang, M.; de Respinis, M.; Frei, H. *Nat. Chem.* **2014**, *6*, 362.
(21) McAlpin, J. G.; Surendranath, Y.; Dincă, M.; Stich, T. A.; Stoian, S. A.; Casey, W. H.; Nocera, D. G.; Britt, R. D. *J. Am. Chem. Soc.* **2010**, *132*, 6882.
(22) Song, F.; Hu, X. *J. Am. Chem. Soc.* **2014**, *136*, 16481.
(23) Walton, R. A. *Coord. Chem. Rev.* **1980**, *31*, 183.

DOI: 10.1021/jacs.6b10307
J. Am. Chem. Soc. 2017, 139, 1878−1884

(24) Schmiers, H.; Friebel, J.; Streubel, P.; Hesse, R.; Köpsel, R. *Carbon* **1999**, *37*, 1965.
(25) Gardner, S. D.; Singamsetty, C. S. K.; Booth, G. L.; He, G.-R.; Pittman, C. U., Jr *Carbon* **1995**, *33*, 587.
(26) Kornienko, N.; Resasco, J.; Becknell, N.; Jiang, C.-M.; Liu, Y.-S.; Nie, K.; Sun, X.; Guo, J.; Leone, S. R.; Yang, P. *J. Am. Chem. Soc.* **2015**, *137*, 7448.
(27) Nakamoto, K. *Infrared and Raman Spectra of Inorganic and Coordination Compounds*, 6th *ed, Part B*; J. Wiley: New York, 2008.
(28) Surendranath, Y.; Kanan, M. W.; Nocera, D. G. *J. Am. Chem. Soc.* **2010**, *132*, 16501.
(29) Moyses Araujo, C.; Doherty, M. D.; Konezny, S. J.; Luca, O. R.; Usyatinsky, A.; Grade, H.; Lobkovsky, E.; Soloveichik, G. L.; Crabtree, R. H.; Batista, V. S. *Dalton Trans.* **2012**, *41*, 3562.
(30) Ogino, H.; Ogino, K. *Inorg. Chem.* **1983**, *22*, 2208.
(31) Xue, Y.; Traina, S. J. *Environ. Sci. Technol.* **1996**, *30*, 1975.
(32) Ma, J. C.; Dougherty, D. A. *Chem. Rev.* **1997**, *97*, 1303.
(33) Schneider, G. F.; Xu, Q.; Hage, S.; Luik, S.; Spoor, J. N. H.; Malladi, S.; Zandbergen, H.; Dekker, C. *Nat. Commun.* **2013**, *4*, 2619.
(34) Chen, Y. W. D.; Santhanam, K.; Bard, A. J. *J. Electrochem. Soc.* **1982**, *129*, 61.
(35) Vaškelis, A.; Jagminien, A.; Tamašauskaité-Tamašiūnait, L. *J. Electroanal. Chem.* **2002**, *521*, 137.
(36) Crandell, D. W.; Ghosh, S.; Berlinguette, C. P.; Baik, M.-H. *ChemSusChem* **2015**, *8*, 844.
(37) Maiyalagan, T.; Jarvis, K. A.; Therese, S.; Ferreira, P. J.; Manthiram, A. *Nat. Commun.* **2014**, *5*, 3949.
(38) Zagal, J. H.; Páez, M. A.; Silva, J. F. In *N4-Macrocyclic Metal Complexes*; Zagal, J. H., Bedioui, F., Dodelet, J.-P., Eds.; Springer: New York, NY, 2006; p 41.
(39) Yeo, B. S.; Bell, A. T. *J. Am. Chem. Soc.* **2011**, *133*, 5587.
(40) Collange, E.; Demirhan, F.; Gun, J.; Lev, O.; Modestov, A.; Poli, R.; Richard, P.; Saurenz, D. In *Perspectives in Organometallic Chemistry*; Screttas, C. G., Steele, B. R., Eds.; The Royal Society of Chemistry: Cambridge, 2003; p 167.
(41) Sosa Torres, M. E.; Saucedo-Vázquez, J. P.; Kroneck, P. M. H. In *Sustaining Life on Planet Earth: Metalloenzymes Mastering Dioxygen and Other Chewy Gases*; Kroneck, P. M. H., Sosa Torres, M. E., Eds.; Springer International Publishing: Cham, 2015; p 1.
(42) Yano, J.; Kern, J.; Yachandra, V. K.; Nilsson, H.; Koroidov, S.; Messinger, J. In *Sustaining Life on Planet Earth: Metalloenzymes Mastering Dioxygen and Other Chewy Gases*; Kroneck, H. P. M., Sosa Torres, E. M., Eds.; Springer International Publishing: Cham, 2015; p 13.

DOI: 10.1021/jacs.6b10307
J. Am. Chem. Soc. 2017, 139, 1878−1884